Stephan KRALL[1*], Christian BAUMANN[1],
Hemant AGIWAL[2], Friedrich BLEICHER[1],
Frank PFEFFERKORN[2]

INVESTIGATION OF MULTILAYER COATING OF EN AW 6060 – T66 USING FRICTION SURFACING

The objective of this research is to investigate observable process changes during multi-layer friction surfacing of EN AW 6060 aluminum, whether for repair, remanufacturing, or new part manufacturing. In this study, friction surfacing was performed with a 10-mm-diameter rod of EN AW 6060 aluminum at spindle speeds ranging from 1000 to 7000 rpm to create up to three layers of 40-mm-long deposits on a substrate of the same alloy. The process forces and layer temperatures were observed. Post-process measurement of flash geometry, layer geometry and microhardness were conducted with the motivation to understand the impact of multi-layer depositions on performance and identifying acceptable conditions required to achieve acceptable build quality. The thickness, deposition and joining efficiency of layers in the multilayer configuration remained consistent. Friction surfacing of EN AW 6060 aluminum allowed for high deposition rates of 9 kg/hr, when compared to other metal additive technologies.

1. INTRODUCTION

Friction surfacing (FS), within the family of friction stir processes, is an emerging solid-state technology that produces fine-grained coatings with excellent corrosion properties [1]. Although the concept of friction surfacing was first mentioned in a patent by Klopstock et al. in 1941 [2], a growing interest has emerged over the last two decades. A schematic illustration of friction surfacing is shown in Fig. 1a. A rotating solid rod is pressed against the substrate under an applied axial load and is traversed along a defined tool-path. Local frictional heating due to the elasto-plastic deformation between the consumable rod and the substrate generates a viscoplastic rubbing interface at the rod tip (Fig. 1b). The material exiting the rubbing interface splits, with a fraction curling away from the substrate (flash) and the rest rolling onto the substrate (coating). The pressure and temperature at the interface between the coating and substrate, as a function of time, enables an interdiffusion process resulting in the formation of a metallurgical bond. By applying a traveling movement, the viscoplastic material is

_____

[1] Institut of Production Engineering and Photonic Technologies, TU Wien, Austria
[2] Department of Mechanical Engineering, University of Wisconsin-Madison, United States
* E-mail: krall@ift.at

deposited onto the substrate surface in a continuous manner. The difference in the tangential velocity to the linear translation velocity of the consumable rod with respect to the substrate was also reported as the cause for deposits to detach [3, 4].
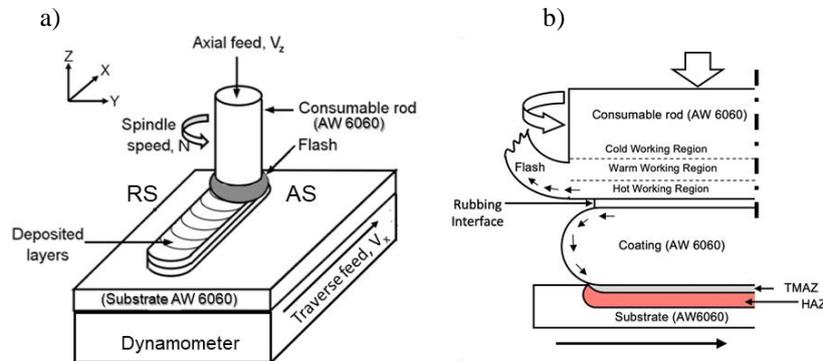
Fig. 1. Schematic of multi-layer friction surfacing (a), thermomechanical events occurring during FS (b)

Friction surfacing uses a consumable rod, part of which becomes the coating, in comparison to the non-consumable tool used in friction stir welding. Additionally, the boundary conditions between friction surfacing and friction stir welding are very different impacting the heat transfer, when material is exposed to atmosphere, and the level of mixing between materials. Significant mixing of materials from both sides of the weld occurs in friction stir welding, whereas the bond between the coating and substrate in friction surfacing is believed to form by a diffusion bonding process with a small amount of relative motion between the surfaces. A closer relative of FS is the Additive Friction Stir process (MELD Manufacturing, Christiansburg, VA, USA) in which the solid feedstock is further constrained by a hollow tool with a shoulder. Unlike in FS, Additive Friction Stir supports the consumable rod along its entire length and adds additional downward pressure on the plastically deformed material as it is rolling onto the substrate [5]. In contrast to FS, the Additive Friction Stir process has a higher deposition rate by avoiding flash material [6].

Friction surfacing has been extensively performed with various combinations of aluminum alloys. The difficulty in weldability of aluminum alloys, makes friction surfacing a viable technology for performing coatings and repairs. Across multiple studies the impact of process parameters in deposition morphology and bonding characteristics for friction surfacing of aluminum alloys has been reported. Sakihama et al. investigated the behavior of 5052 aluminum alloy in FS with different rotational and traverse speeds [7]. Gandra et al. studied the effect of process parameters, such as, axial force, rotation and travel speed for two different aluminum alloys, AA 6082-T6 coatings on AA 2024-T3 substrates [8]. Kallien et al. performed a detailed experimental study of the process temperatures during FS of dissimilar aluminum alloys [9]. In general, the thickness and width of coatings decreased with increase in traverse speeds and axial pressures. The joining efficiency was found to improve with reduction in axial pressures and rotation speeds. With peak temperatures during friction surfacing staying below the solidus, the coated structures have better mechanical properties compared to the fusion based deposition methods, with tensile strength of higher than 75% of the base material [10]. The material flow during friction

surfacing of aluminum alloys has been described to be similar to simple shear flow [11]. The high strain rates and temperature conditions lead to discontinuous dynamic recrystallization of the deformed material. In general, this results in higher hardness in coatings. Yu et al. [12] attributed the reduction in grain size and recrystallization for improvement in corrosion resistance in deposited coatings. Efforts have also been put to understand the thermomechanical evolution of the process by using computational methods to conduct phase-field temperature simulations. Pirhayati et al. [13] studied the impact of traverse speed on incubation and recrystallization time during friction surfacing of AA 2024 aluminum alloys. The authors reported a reduction decrease in rate of plastic deformation with increasing traverse speeds. Higher temperatures in advancing side of the coating has also been reported in literature [14].

In recent years friction surfacing has also been deployed to produce multilayer coatings. Batchelor et al. [15] studied the effect of metal type on multilayer friction surfacing using consumable rods made of brass, aluminum, and stainless steel on mild steel substrates. They were only able to bond stainless steel on the mild steel substrates. Cause the thermal conductivity of the coating material is one of the important factors to ensure a good deposit. Tokisue et al. [16], deposited AA2017 alloy on AA5052 substrates. They reported a higher efficiency of deposit in multilayer configuration compared to monolayer coatings. Multilayer friction surfacing can involve significant reheating of previous layers on heat treatable alloys such as AA2014 when deposited over AA5083 [17]. They reported over-aging of strengthening precipitates due to the process. Multilayer friction surfacing has also been used to produce functionally graded coatings and metal matrix composites. Gandra et al. [18] used multilayered coatings to enable tailored coating compositions to achieve predefined gradients. They reinforced SiC particles in AA6083 rods in increasing concentration per layer. In another study Karthik et al. [19], were able to uniformly disperse reinforced titanium particles in AA5083 consumable rods, and deposited on substrates of the same material. They reported formation of very fine equiaxed grains and well-dispersed second phase particles.

The literature review has shown the feasibility of friction surfacing as an additive process using aluminum alloys, however, to the best of authors' knowledge, there still lies a gap in understanding the impact of processing parameters on the dynamics and performance of the process.

In this study friction surfacing was conducted using AW 6060 consumable rod and substrate. A comprehensive range of process parameters were chosen and their effects on the thermomechanical events of the process were studied using process signatures such as deposition morphology, forces and temperature profiles. The acceptable processing condition was then used for multi-layer configuration. This study is also the first to perform multi-layer friction surfacing with the aforementioned material combination.

2. MATERIALS AND METHODS

The experimental setup of the conducted FS experiments on a 3-axis CNC milling machine (HAAS, VF2, USA) is shown in Fig. 2. The consumable rods with a diameter of 10 mm were clamped in a normal collet chuck holder and had a protruding length

of 40 mm. The machining center is equipped with a dynamometer on the machine tool table, using a mounting plate, to measure process forces. The workpiece is mounted atop the three-axis piezoelectric force dynamometer (Kistler model 9139AA, Switzerland).

The photo measurements of the flash formation were made with a digital single-lens reflex (DSLR) camera (NIKON model D750, Japan) in series image capture mode. The photos were captured with an image size of 6016×4016 pixels at an exposure time of 1/20 seconds. Other parameters were set to aperture of F/8, and ISO value of 500. The DSLR was installed inside the machine enclosure to observe the process.

Furthermore, temperature measurement was done for the first layer. The maximum temperature to be expected from the literature in the FS process serves the basis to select suitable sensors. For aluminum, this is lower than the solidus temperature FS [1]. A resistance temperature detector (RTD) sensor PT 1000 (TE Connectivity, Germany) which uses a thin film platinum resistor was used to measure the temperature behavior. This single sensor was embedded in the substrate with a distance to the top surface of 0.1 mm. During the FS process the deposition was run over the sensor. The used RTD sensor is able to measure temperatures in a range of –50 to 600°C.

Due to the process dynamics in combination with a high local temperature resolution, miniature PT1000 with a size of 1.2×4.0 mm was selected. The temperature sensors must be supplied with 0.3 mA via a constant current source. This is necessary so that the temperature-proportional resistance value, which is detected by the AD converter of the microcontroller as a voltage drop at the sensor, can be properly calculated back to the temperature value. The resistance value of the PT-1000 about 1000 Ω at 0°C and about 3140 Ω at 600°C. The exact relationship between resistance value and temperature is provided by a 2nd degree polynomial fit [20]. In order to detect the voltage-drop, an OPV circuit with an amplification factor of 5 is used downstream of the A/D converter. After amplifying the measurement signal by a factor of 5, this results in a theoretical measurement error of ±0.83°C.

Fig. 2. Experimental setup for friction surfacing tests at TU Wien

Experiments were conducted using EN AW-6060 – T66 5-mm-thick aluminum sheet substrate (EMERUS, Bosnia & Herzegovina), with a tensile strength of R_m 228 MPa and a mean hardness value of the 68 HV1. The EN AW-6060 – T66 aluminum rod of 10 mm diameter (ALCOMET AD, Bulgaria) has a tensile strength R_m of 215 MPa and a mean hardness value of 78 HV1. Table 1 shows the chemical compositions of the aluminum substrate and rod which were used for all performed FS experiments.

Table 1. Composition of EN AW-6060 – T66 substrate and consumable rod

EN AW-6060 – T66 Standard		Substrate	Consumable rod
Element	Weight%	Weight%	Weight%
Silicon	0.30–0.60	0.4404	0.54
Iron	0.10–0.30	0.1539	0.25
Copper	0.10 max	0.0001	0.00
Manganese	0.10 max	0.0022	0.01
Magnesium	0.35–0.60	0.4063	0.53
Zinc	0.15 max	0.0069	0.01
Titanium	0.10 max	0.0088	0.01
Chromium	0.05 max	0.0005	0.00
Aluminum	Balance	Balance	Balance

The process kinematics of the friction surfacing process are shown in Fig. 3. In Fig. 3a the toolpath of the consumable rod is shown in terms of x and z movement and derived from this Fig. 3b shows a simplified velocity-time-graph. Starting the FS-process the consumable rod rotates with a defined spindle speed (n) and is positioned above the point of contact (z_p). Next, the movement of the spindle with its clamped consumable rod with a constant plunge rate (v_{zp}) in z-direction starts. After a dwell time (t_{dwell}) the rod is traversed along the substrate in x-direction with a lateral traverse feed rate (v_x) and a constant axial feed rate (v_z). The dwell time is defined as the time between the plunging and the start of the transverse motion. The cantilever length of the rod of all deposits (l_d), measured from the collet chuck, was 40 mm. The cantilever length for all the consumable rods used in this study forms a good compromise in terms of mechanical stability. Wobbling or bending effects are kept low with a 4-to-1 ratio between the length and the diameter of the rod. The deposition length is limited to 40 mm. With an axial feed rate in the range of 440 to 1100 mm/min within an axial movement of 23 mm, only 17 mm still remain for flash formation. By that, the flash height limits the length of deposition (Fig. 3c). While the non-continuous nature of this process may limit its use in additively manufacturing new parts, it can be performed on any CNC mill to perform repairs or add small features. All materials were degreased before the tests with pure alcohol.

In Fig. 3c the motion of the rod in v_x and v_z during the traverse motion is visible and the evolution of the deposition and the flash height over time can be investigated.

Experiments starts with a parameter variation based on previous experiments. The test parameters are shown in Table 2. The parameter study was carried out for spindle speeds in the range 4000–7000 rpm and for traverse feed rates v_x of 800–2000 mm/min. After evaluating the deposited layers of step for low to middle speeds, in a second step the spindle speed was limited to 5000 rpm due to quality aspects of the deposited layers.
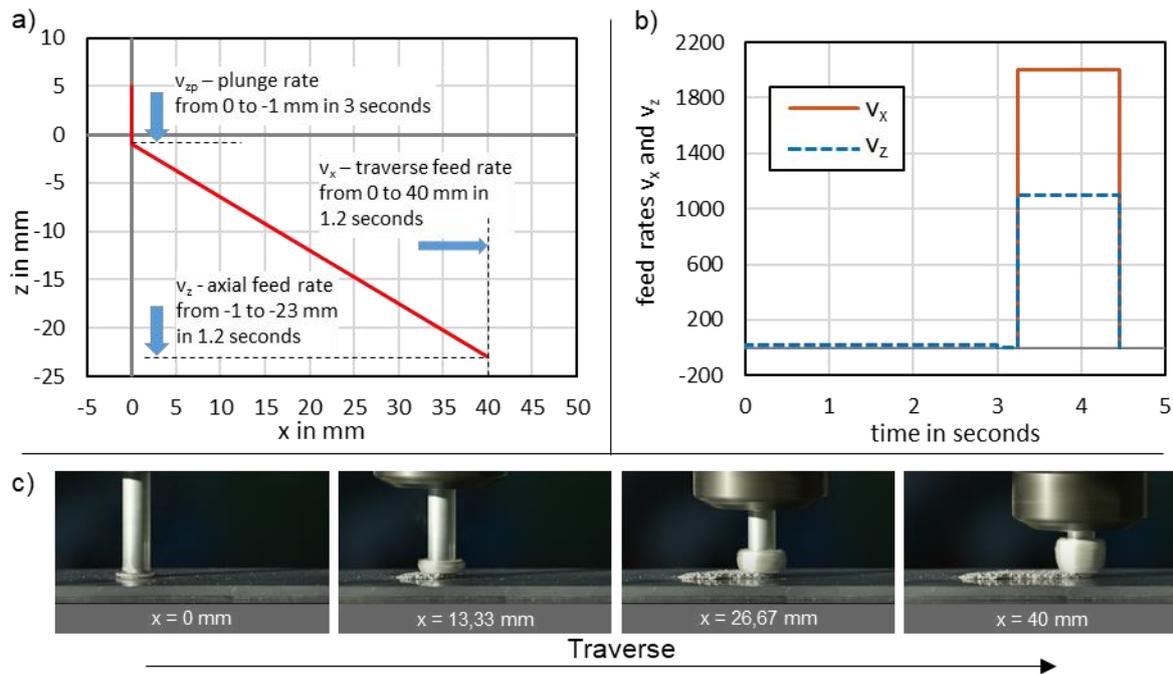
Fig. 3. Process kinematics for FS: a) consumable rod path, b) rod velocities, c) evolution of FS deposit

Table 2. Friction surfacing parameters used in the parameter study (for EN AW-6060 – T66)

Spindle speed, n	4000–7000 rpm
Lateral traverse feed rate, v_x	800–2000 mm/min
Axial feed rate, v_z	440–1100 mm/min
Initial plunge, z_p	1 mm
Plunge rate, v_{zp}	20 mm/min
Dwell at end of plunge, t_{dwell}	0.25 seconds
Length of deposit, l_d	40 mm

To evaluate the quality of the deposited layer, transverse cross-sections of the samples were made. The specimens were extracted from the center of the deposited layer, in the lateral y-z-plane (perpendicular to the traverse direction) to observe the steady state region. If the process is stabilized in the z-force, a so-called steady state region is reached. The cross-sectional specimens were then ground successively with 240, 400, 600, 800, 1200, and 2500 grit SiC paper, followed by polishing with 6 µm and 1 µm diamond slurry.

Micro-indentation tests were conducted with a mobile microhardness tester Kraut-kramer MIC 20 (General Electric, USA) using a Vickers diamond indenter in conjunction with its HV1 (load = 9.81 N). The hardness measurements were performed within the produced layers from the top of the coating across the interface into the substrate.

Beside the evaluation of deposition morphology through cross-section and hardness profiles of the deposited material for single and multi-layer, the metrics according to Gandra et al. [21] were used to quantitatively describe the layer properties. In addition to these metrics, a new indicator was defined to describe the amount of bonded material after deposition (B_{rate}). For the most applications the unbonded edges of the layers have to be

removed afterwards to create a functionally acceptable geometry. The B_{rate} can be determined by multiplying the deposition rate and joining efficiency. The joining efficiency describes the ratio between the bonded width (w_b) and the total width of deposition (w_d) and indicastes the part of the deposited area that is effectively joined to the substrate.

$$B_{rate} = D_{rate} \cdot J_{eff} \qquad (1)$$

where: D_{rate} – deposition rate, J_{eff} – joining efficiency.

3. RESULTS AND DISCUSSION

In this section the deposited FS layers are investigated and a comparison between the properties of a single and a multi-layer were done. In detail a discussion on the deposition morphology, variations in process dynamics and the properties in microstructure were presented.

3.1. SINGLE LAYER DEPOSITION

In order to classify the results of the deposited layer, a visual evaluation of deposition morphology was done to assess the quality. The uniformity in height and width of each layer and the layer adhesion was evaluated. The latter was done using a feeler gauge to inspect possible air gaps. The results of this evaluation metrology are shown in Fig. 4.

In addition to visual inspections, the implemented dynamometer was used to visualize the forces of the FS process. It is characteristic for this kind of process that the normal force is immediately rising when the consumable rod touches the substrate. In Fig. 4a an exemplary FS-process for aluminum is shown. Within the initial pre-heating stage of friction surfacing, frictional heat due to contact is the major energy source, which is proportional to the applied pressure. The temperature of material continues to rise and combined with high strain rates, the stick-slip conditions vary continuously as the material begins to plastically deform. Since plastic deformation depends on the shear stresses and internal energy stored within the heated rod the dependence on frictional pressure reduces. At this stage the process force starts to drop, till the entire rod face has completely reached the plastic deformation stage and the forces stabilize, entering the steady state regimen.

The *z*-force is the highest force in the FS-process, with the peak forces attained at the initial cold contact. Figure 4b indicates the maximum value of contact force while plunging compared to the rotational speed. The numbers represent an average value of all parameter sets at same speeds.

In Fig. 4c the mean average signal of the steady state force for each parameter set is shown. Parameters which lead to a usable layer are indicated in green, appropriate layer with some lack in homogenous layer structures (height and width) in orange and not-usable parameters are colored in red. It can be seen, that a minimum value of the steady state fore

of approximately 1200 N is needed to achieve a good bonding condition. To indicate the difference in layer quality, Fig. 4d shows exemplary some pictures of the different layers classified by its quality.

As a result, it can be seen that low rotational speeds in combination with low feed rates lead to an unsuitable deposition result and bonding behavior. By increasing the speed and feed the homogeneity of the layer increases. Each layer decreases in height by increasing the feed rate. At a speed of 5000 rpm in combination with higher feed rates, the quality of the deposited layer increases.
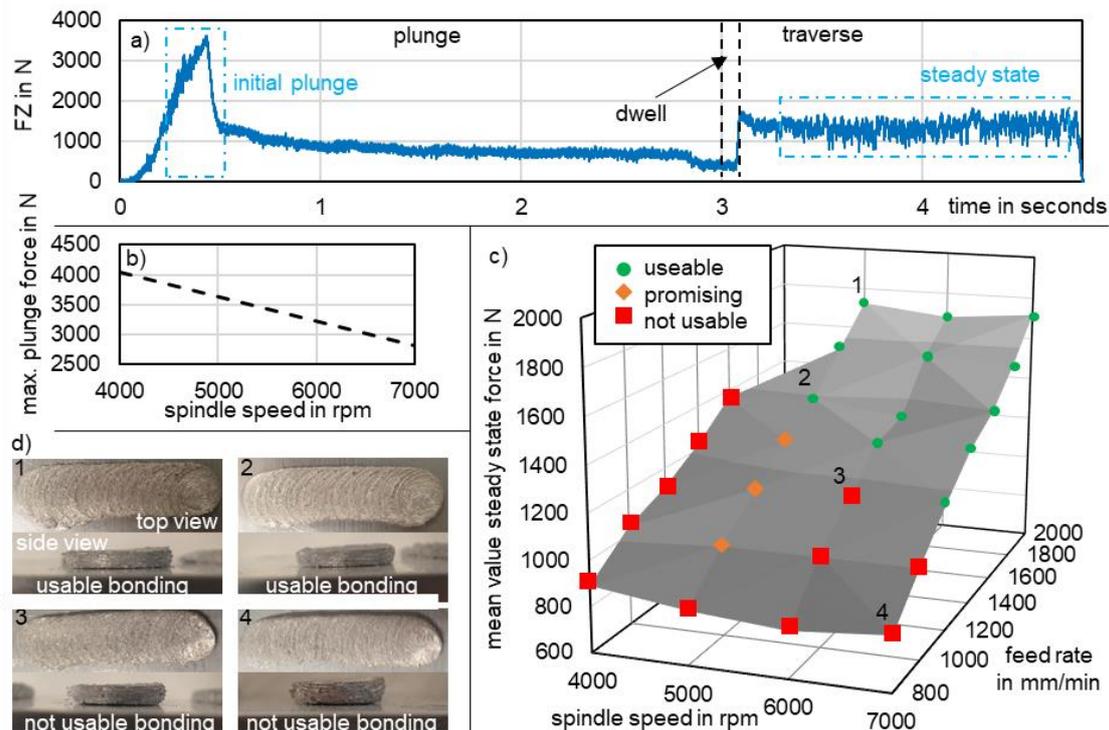
Fig. 4. Results of the parameter study: a) exemplary FS-process for aluminum, b) maximum plunge force, c) mean average steady state force, d) detailed images of usable and not usable bondings

Based on the shown parameter tests, Table 2 lists the most promising parameter set for further FS experiments. The used parameter set, represented as point 1 in Fig. 5, showed the best properties in terms of layer adhesion and productivity.

In Fig. 5 a cross-section of a single layer using the parameters of Table 3 is displayed. As it can be seen, the layer can be sectioned into an unbonded and a bonded part. Most of the unbonded region is on the retreating side. By measuring the total width (w_d) and the bonded width (w_b) of deposition, the percentage of the bonded surface, joining efficiency (J_{eff}), can be calculated as about 58%. These unbonded regions need to be machined off for better mechanical and corrosion performance of the coatings. The deposition efficiency (D_{eff}) for the shown single layer can be calculated to 70%, the coating efficiency (C_{eff}) to 40% (Table 4). Thus, the major fraction of the plastically deformed material goes into the flash.
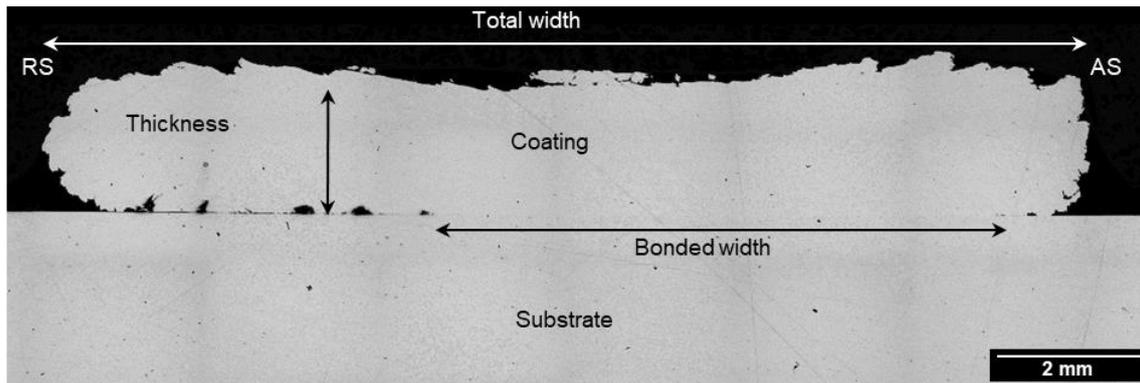
Fig. 5. Cross-sectional view of deposit for single layer friction surfacing of EN AW 6060 – T66

Next to cross-sections, the normal forces in *z*-direction of two identical FS parameter tests are shown in Fig. 6. Similar to the force plot shown in Fig. 4 the process forces during deposition of a single layer can be split up in three-time segments (plunge, dwell and traverse). The measured *z*-force during plunging and in the steady-state was calculated from two experiments for one single layer. The results are shown in two bar plots in Fig. 6. What is also striking is that both force plots over time shows only a small deviation in the traverse segment.
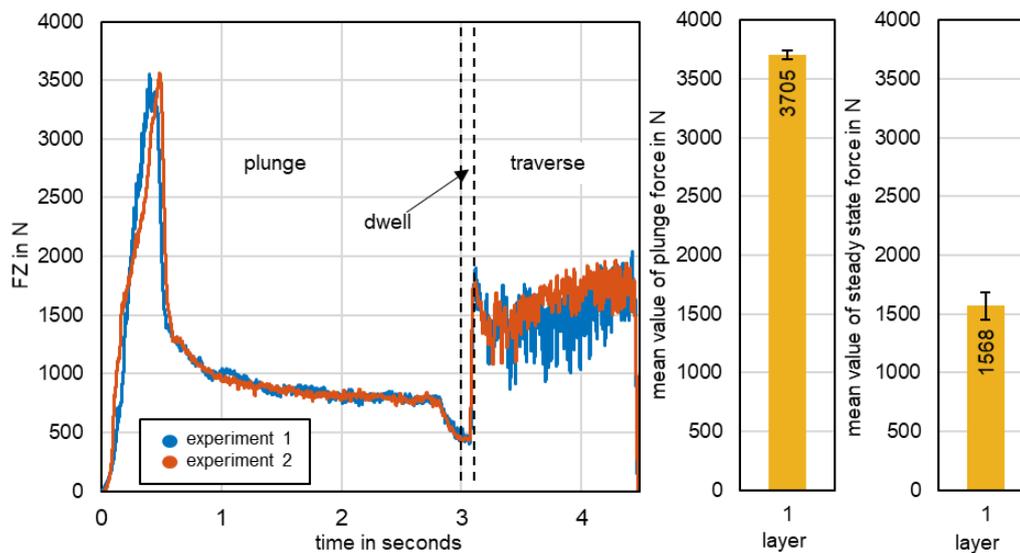
Fig. 6. Measured process force in z-direction for single layer deposition of EN AW 6060 – T66

In order to obtain the temperature behavior while FS a single RTD sensor was implemented in the substrate close to the surface. As the temperature is influenced by the heat flux, the temperature difference due to heat conduction need to be added to the measured sensor data to obtain the surface temperature. As aluminum has a high thermal conductivity and the difference in height is about 0.1 mm, therefore, the difference between measured data and the surface temperature can be neglected. In Fig. 7 the temperature data of the RTD sensor is shown.
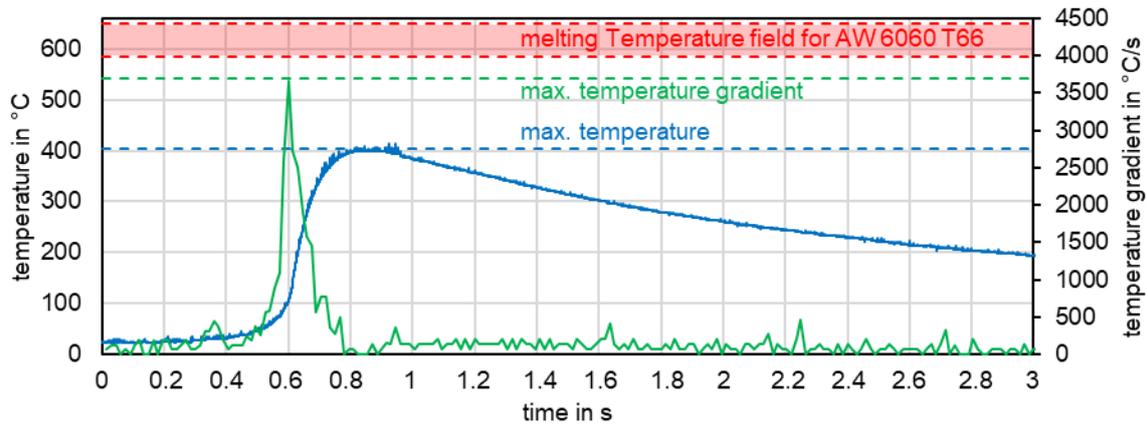
Fig. 7. Measured temperature of the substrate during single layer deposition of EN AW 6060 – T66

From this dataset the temperature gradient was calculated by dT/dt (green). It is clearly visible, that the maximum measured temperature is below the liquidus area of AW 6060 T66. The peak temperature achieved during the deposition is 405°C, which is 62–69% of the solidus temperature for EN AW 6060 – T66. The temperature gradient shows a value of about 3700°C/s and indicates that FS is a highly dynamic process in terms of temperature. The cooling behavior indicates an exponential decay. Thus, a local heat zone is still retained for a short time.

3.2. MULTI-LAYER DEPOSITION

Table 3. Friction surfacing parameters chosen for multi-layer deposition (for EN AW-6060 – T66)

Spindle speed, n	5000 rpm
Lateral traverse feed rate, v_x	2000 mm/min
Axial feed rate, v_z	1100 mm/min
Initial plunge, z_p	1 mm
Plunge rate, v_{zp}	20 mm/min
Dwell at end of plunge, t_{dwell}	0.25 seconds
Length of deposit, l_d	40 mm

To evaluate a multi-layer FS process, the most promising parameter from the single-layer process set was selected. The parameters used for multi-layer deposition are listed in Table 3. For multilayered coatings, three layers were deposited using identical process parameters. The rods were plunged at the same position for all three layers. In order to have the same initial conditions for all layers, a cooling time was considered to start at room temperature. Similar to single layer depositions, no shielding gas was used and no post processing of coatings (e.g., machining, polishing) was performed.

Figure 8 shows a cross-section of multiple layers, it can be observed that the total and bonded widths as well as the thickness of each layer are similar in all layers. These measurements have been summarized in Table 4. This leads to a relatively consistent joining

efficiency. By observing the coating efficiency (C_{eff}), which reflects the fraction of the consumed rod that is actually bonded to the substrate, a nearly constant behavior over the three layers is seen (Table 4). This indicates that the deposition process is not changing and process parameters do not have to be adapted layer wise in order to create multi-layer deposits. Despite the good coating efficiency some unbonded areas or cavities between the substrate and layer one, as well as between the layers were observed. This can be due to an undefined surface roughness and oxides on top of each layer. In order to avoid these kinds of defects, machining of the top surface of each deposited layer can be performed.
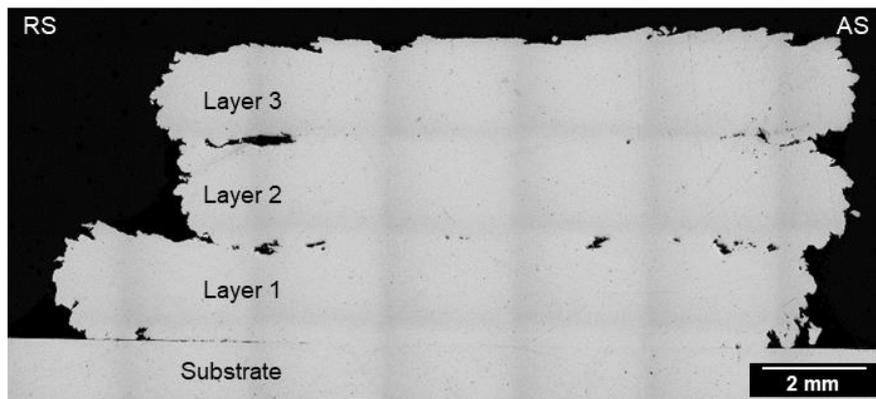
Fig. 8. Cross-sectional view of multi-layer depositions of EN AW 6060 – T66 by friction surfacing

In Fig. 9 the change in flash height as a function of deposition length for all three layers is shown. The slope of flash height runs similarly to the axial feed rate (v_z). When plunging, the flash height has a higher slope than the feed rate. In the traverse region it is opposite. This difference is attributed to the curling of the flash and an increase in thickness as the deposition progresses. This linear slope of flash height for all three layers, as a function of time, is similar. This suggests that the flash height is not influenced by small process changes which can be seen in Table 4.
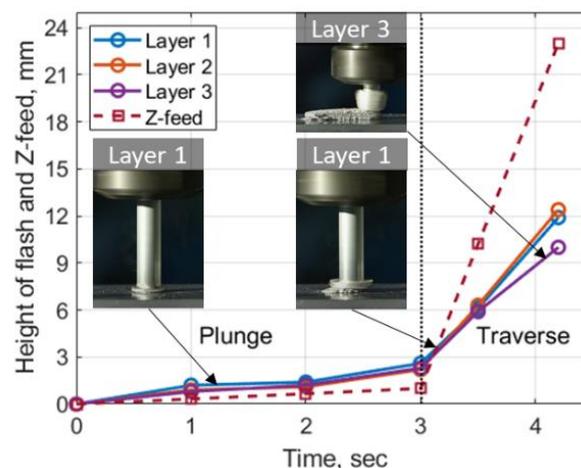
Fig. 9. Flash height as a function of time for multi-layered deposits of EN AW 6060 – T66

In Fig. 10 the axial (z) forces for multi-layer deposition of all three layers have been plotted. After the 1st layer the peak forces while plunging are delayed. As a result of the high surface-roughness and a starting ramp of the deposition height of the 1st layer, the consumable rod has no solid contact with the 1st layer and begins to wobble (Fig. 10) at start for the 2nd and the 3rd layer. This can be observed in the x and y forces which are up to 1400 N. Subsequently, no fast warm up in the consumable rod as well as in the substrate takes place and therefore, the plunging stage is unstable. The 2nd and the 3rd layers do not show a typical small high rising single peak like the first layer. After plunging (about 3 seconds) and beginning the transverse motion, the forces in x, y and z stabilized and a visible steady-state with higher z forces (approximately 400 N more) was observed for the 2nd and the 3rd layers. For each new layer a new consumable rod, with the same size, was used and plunged at the same starting point. Between each deposition, the layers were allowed to cool down to room temperature before depositing the next one.
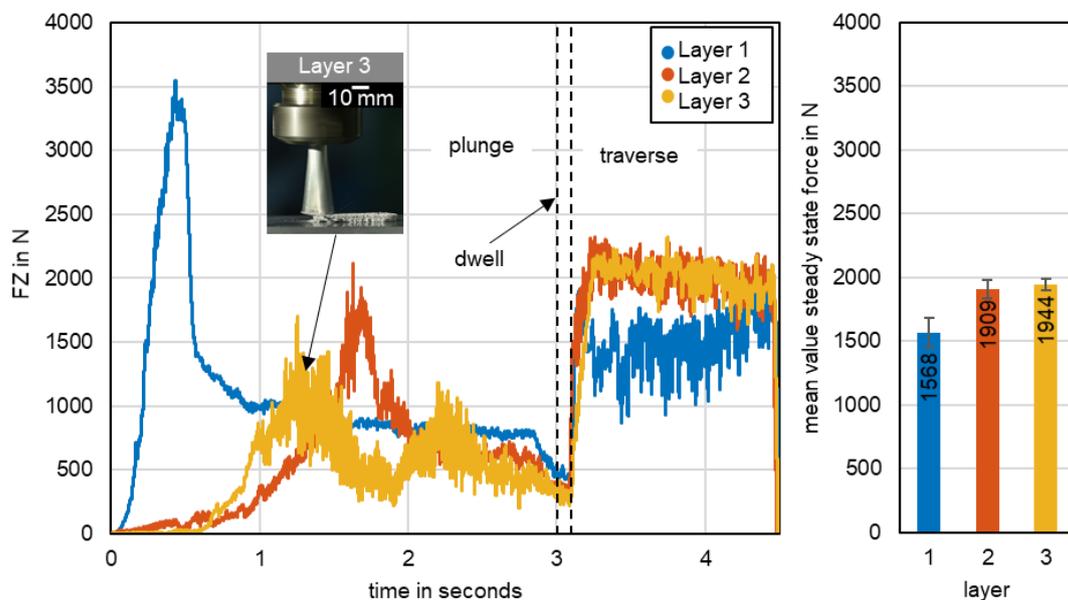
Fig. 10. Z-forces for each layer in a multi-layered deposition of EN AW 6060 – T66 using friction surfacing

Figure 11 shows the microhardness measurements for the multi-layer friction surfacing process. The substrate has a mean bulk hardness value of 68 HV1. It can be seen that the hardness of the substrate decreases in the heat affected zone of the substrate. The deposited layers have an average hardness of 56 HV1 (measured close to the process centerline), which is 29% lower than the initial hardness of the consumable rod. Research on friction surfacing of steels has shown that the deposited layers have higher hardness than the consumable rod, which is primarily due to the Hall-Petch effect, i.e., increasing hardness with decreasing grain size [22, 23]. For aluminum a decrease in hardness is also shown by Gandra [10], where the layer presents a refined microstructure, but the loss of the T6 initial heat treatment leads to a 15% hardness decrease compared to the rod in as-received condition. Table 4 shows a summary of the measured physical quantities and calculated performance metrics according to [21] that are discussed in this section.
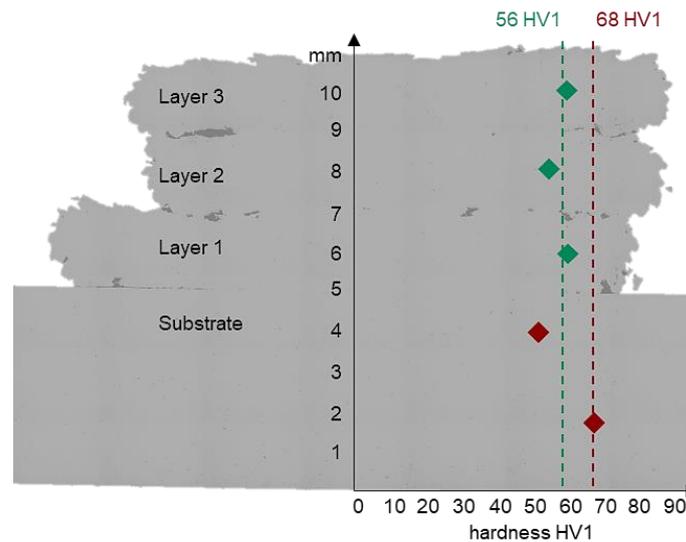
Fig. 11. Microhardness (HV1) profile for multi-layered friction surfacing of EN AW 6060 – T66

Table 4. Measured physical quantities for multi-layer deposition

		Layer		
	Units	1	2	3
Deposition morphology and process variables				
Total width of deposition, w_d	mm	15.01	13.08	13.70
Bonded width of deposition, w_b	mm	8.68	8.37	8.33
Thickness of deposition, h_d	mm	2.00	2.00	2.04
Steady state axial force, F_{steady}	N	1540	1982	1993
Performance metrics				
Consumption rate, C_{rate}	kg/hr	14.00	14.00	14.00
Deposition rate, D_{rate}	kg/hr	9.74	8.47	9.04
Deposition efficiency, D_{eff}	%	69.6	60.5	64.6
Joining efficiency, J_{eff}	%	57.8	64.0	60.8
Coating efficiency, C_{eff}	%	40.2	38.8	39.3
Bonding rate, B_{rate}	kg/hr	5.63	5.42	5.50

4. SUMMARY

Friction surfacing was performed using consumable rods and substrates made of EN AW 6060 – T66 to produce single and multi-layered coatings at constant process parameters. All depositions were performed using position control. The observations of various in-process measurements and post process characterization can be summarized as:

- An extensive study of process parameters was conducted to obtain conditions which produce acceptable morphology and interface for the coatings. It was observed that for the alloy and rod diameter in this study, a rotation speed of higher than 5000 rpm and traverse rates greater than 1600 mm/min were acceptable.

- A minimum value of the steady state force of approximately 1200 N is needed to achieve a good bonding condition.
- Due to the high traverse rates friction surfacing was able to deposit coatings at deposition rates of 9 kg/hr.
- Temperature profiles during friction surfacing were recorded using RTD sensors and a peak temperature close to 400°C (~ 70% of solidus) was observed.
- Large temperature gradients during friction surfacing were observed, which lead to the loss of T6 heat treatment condition in the base metal. This resulted in reduction of hardness in the deposited material.
- Multilayer deposits using acceptable condition obtained from single layer deposits were performed. The thickness, deposition and joining efficiency remained fairly consistent across the three layers.
- The process dynamics during traverse motion were consistent across all layers. However, the presence of oxides and uneven surface, the subsequent layers experienced wobbling of the consumable rod during the plunging stage.

This study shows that the friction surfacing parameters don't need to be adjusted even after the second layer of EN AW 6060 – T66 is deposited. As most of the material goes into flash during the FS process a need to find methods for reusing or recycling the material evolved as flash is logical. The friction surfacing process as studied in this work is accessible to anybody with a CNC mill and is very well suited for repairs, remanufacturing, and the addition of small features. In addition, due to its small size the consumable rod can access inside pockets.

ACKNOWLEDGEMENTS

REFERENCES

[1]   GANDRA J., KROHN H., MIRANDA R.M., VILACA P., QUINTINO L., DOS SANTOS J.F., 2014, *Friction Surfacing – A Review*, Journal of Materials Processing Technology, 214, 5, 1062–1093.

[2]   KLOPSTOCK H., 1941, *An Improved Method of Joining or Welding Metal*s, Patent Specification Ref. 572789.

[3]   BEDFORD G.M., VITANOV V.I., VOUTCHKOV I.I., 2001, *On the Thermo-Mechanical Events During Friction Surfacing of High Speed Steels*, Surface and Coatings Technology, 141/1, 34–39.

[4]   RAFI H.K., PHANIKUMAR G., RAO K.P., 2011, *Material Flow Visualization During Friction Surfacing*, Metallurgical and Materials Transactions A, 42/4, 937–939.

[5]   PHILLIPS B.J., AVERY D.Z., LIU T., RODRIGUEZ O.L., MASON C.J.T., JORDON J.B., BREWER L.N., ALLISON P.G., 2019, *Microstructure-Deformation Relationship of Additive Friction Stir-Deposition Al–Mg–Si*, Materialia 7, 100387, ISSN 2589–1529.

[6]   KHODABAKHSHI F., GERLICH A.P., 2018, *Potentials and Strategies of Solid-State Additive Friction-Stir Manufacturing Technology: A Critical Review*, Journal of Manufacturing Processes, 36, 77–92, ISSN 1526–6125.

[7]   SAKIHAMA H., TOKISUE H., KATOH K., 2003, *Mechanical Properties of Friction Surfaced 5052 Aluminum Alloy*, Materials Transactions, 44/12, 2688–2694.

[8]   GANDRA J., PEREIRA D., MIRANDA R.M., VILAÇA P., 2013. *Influence of Process Parameters in the Friction Surfacing of AA 6082-T6 Over AA 2024-T3*, Procedia CIRP, 7, 341–346.

[9]   KALLIEN Z., RATH L., ROOS A., KLUSEMANN B., 2020, *Experimentally Established Correlation of Friction Surfacing Process Temperature and Deposit Geometry,* Surface and Coatings Technology, 397, 126040.

[10]   GANDRA J., PEREIRA D., MIRANDA R.M., SILVA R.J.C., VILAÇA P., 2013, *Deposition of AA6082-T6 Over AA2024-T3 by Friction Surfacing-Mechanical and Wear Characterization*, Surface and Coatings Technology, 223, 32–40.

[11]   SUHUDDIN U., MIRONOV S., KROHN H., BEYER M., DOS SANTOS J.F., 2012, *Microstructural Evolution During Friction Surfacing of Dissimilar Aluminum Alloys*, Metallurgical and Materials Transactions A, 43/13, 5224–5231.

[12]   YU M., ZHANG Z., ZHAO H., ZHOU L., SONG X., 2019, *Microstructure and Corrosion Behavior of the Ultra-Fine Grained Aluminum Coating Fabricated by Friction Surfacing*, Materials Letters, 250, 174–177.

[13]   PIRHAYATI P., JAMSHIDI AVAL H., 2020, *Phase-Field Microstructure Simulation During Aluminum Alloy Friction Surfacing*, Surface and Coatings Technology, 402, 126496.

[14]   BARARPOUR S.M., JAMSHIDI AVAL H., JAMAATI R., 2019, *Modeling and Experimental Investigation on Friction Surfacing of Aluminum Alloys*, Journal of Alloys and Compounds, 805, 57–68.

[15]   BATCHELOR A.W., JANA S., KOH C.P., TAN C.S., 1996, *The Effect of Metal Type and Multi-Layering on Friction Surfacing*, Journal of Materials Processing Technology, 57/1–2, 172–181.

[16]   TOKISUE H., KATOH K., ASAHINA T., USIYAMA T., 2006, *Mechanical Properties of 5052/2017 Dissimilar Aluminum Alloys Deposit by Friction Surfacing*, Materials Transactions, 47/3, 874–882.

[17]   DILIP J.J.S., JANAKI RAM G.D., 2013, *Microstructure Evolution in Aluminum Alloy AA 2014 During Multi-Layer Friction Deposition*, Materials Characterization, 86, 146–151.

[18]   GANDRA J., VIGARINHO P., PEREIRA D., MIRANDA R.M., VELHINHO A., VILACA P., 2013, *Wear Characterization of Functionally Graded Al–Sic Composite Coatings Produced by Friction Surfacing*, Materials & Design, 52, 373–383.

[19]   KARTHIK G.M., JANAKI RAM G.D., KOTTADA R.S., 2016, *Friction Deposition of Titanium Particle Reinforced Aluminum Matrix Composites*, Materials Science and Engineering A, 653, 71–83.

[20]   Datasheet of NB-PTCO-012 (PT1000) TE connectivity, website: *https://www.te.com/deu-de/product-NB-PTCO-012.html*, download: 10.01.2022.

[21]   GANDRA J., MIRANDA R.M., VILACA P., 2012, *Performance Analysis of Friction Surfacing*, Journal of Materials Processing Technology, 212, 1676–1686.

[22]   PULI R., JANAKI RAM G.D., 2012, *Dynamic Recrystallization in Friction Surfaced Austenitic Stainless Steel Coatings*, Materials Characterization, 74, 49–54.

[23]   GUO D., KWOK C.T., CHAN S.L.I., 2019, *Spindle Speed in Friction Surfacing of 316L Stainless Steel – How it Affects the Microstructure, Hardness and Pitting Corrosion Resistance*, Surface and Coatings Technology, 361, 324–341.